Charge and spin structures of a $d_{x^2-y^2}$ superconductor in the proximity of an antiferromagnetic Mott insulator

F. F. Assaad*
Department of Physics, University of California, Santa Barbara, California 93106-9530

M. Imada
Institute for Solid State Physics, University of Tokyo, 7-22-1 Roppongi, Minato-ku, Tokyo 106, Japan

D. J. Scalapino
Department of Physics, University of California, Santa Barbara, California 93106-9530
(Received 10 June 1997; revised manuscript received 15 September 1997)

To the Hubbard model on a square lattice we add an interaction W that depends upon the square of a near-neighbor hopping. We use zero-temperature quantum Monte Carlo simulations on lattice sizes up to 16×16, to show that at half-filling and constant value of the Hubbard repulsion, the interaction W triggers a quantum transition between an antiferromagnetic Mott insulator and a $d_{x^2-y^2}$ superconductor. With a combination of finite-temperature quantum Monte Carlo simulations and the maximum entropy method, we study spin and charge degrees of freedom in the superconducting state. We give numerical evidence for the occurrence of a finite-temperature Kosterlitz-Thouless transition to the $d_{x^2-y^2}$ superconducting state. Above and below the Kosterlitz-Thouless transition temperature, T_{KT}, we compute the one-electron density of states $N(\omega)$, the spin relaxation rate $1/T_1$, as well as the imaginary and real part of the spin susceptibility $\chi(\vec{q},\omega)$. The spin dynamics are characterized by the vanishing of $1/T_1$ and divergence of Re $\chi(\vec{q}=(\pi,\pi),\omega=0)$ in the low-temperature limit. As T_{KT} is approached $N(\omega)$ develops a pseudogap feature and below T_{KT} Im $\chi(\vec{q}=(\pi,\pi),\omega)$ shows a peak at finite frequency. [S0163-1829(97)04848-0]

I. INTRODUCTION

The motivation of this work is to examine the competition and relationship between an antiferromagnetic Mott insulating state and a $d_{x^2-y^2}$ superconducting state in two dimensions using numerical simulations. In particular, we are interested in the interplay of these two states and the remnant of the antiferromagnetic correlations in the superconducting state. We will see that significant antiferromagnetic fluctuations remain in the $d_{x^2-y^2}$ superconducting state. The antiferromagnetic Mott insulator is well described by the ground state of the half-filled Hubbard model on a square lattice with on-site Coulomb repulsion U and nearest-neighbor single-particle hopping t.[1] To this model, we add an extra term W that depends upon the square of the single-particle nearest-neighbor hopping. Staying at half-band filling and constant value of U, we have previously shown that we can generate a quantum transition as a function of the coupling strength W between an antiferromagnetic Mott insulating state and a $d_{x^2-y^2}$ superconducting state.[2] Technically, with the system at half-filling, and with our particular choice of W, we encounter no fermion sign problem in the quantum Monte Carlo (QMC) simulations. Large lattice sizes and low temperatures may thus be reached without loss of precision. While there are various ways to justify the form of the microscopic Hamiltonian, we view the choice of the interaction more formally as a means of inducing the desired quantum transition. In fact, one of the reasons for choosing this form is that it has a simple Hubbard-Stratonovitch representation that is useful in constructing the Monte Carlo simulation. Although the formalism with the W term may be extended to any lattice structure, we study here the two-dimensional system on a square lattice.

The basic half-filled Hubbard model that we will study has the Hamiltonian

$$H_{tU} = -\frac{t}{2}\sum_{\vec{i}} K_{\vec{i}} + U\sum_{\vec{i}} (n_{\vec{i},\uparrow} - \tfrac{1}{2})(n_{\vec{i},\downarrow} - \tfrac{1}{2}) \qquad (1)$$

with the hopping kinetic energy

$$K_{\vec{i}} = \sum_{\sigma,\vec{\delta}} (c^{\dagger}_{\vec{i},\sigma} c_{\vec{i}+\vec{\delta},\sigma} + c^{\dagger}_{\vec{i}+\vec{\delta},\sigma} c_{\vec{i},\sigma}). \qquad (2)$$

Here, $c^{\dagger}_{\vec{i},\sigma}$ ($c_{\vec{i},\sigma}$) creates (annihilates) an electron with the z component of spin σ on site $\vec{i}$, $n_{\vec{i},\sigma} = c^{\dagger}_{\vec{i},\sigma} c_{\vec{i}\sigma}$, and $\vec{\delta} = \pm\vec{a}_x, \pm\vec{a}_y$ where $\vec{a}_x$, $\vec{a}_y$ are the lattice constants. The energy will be measured in units of t. We consider the boundary conditions

$$c_{\vec{i}+L\vec{a}_x,\sigma} = \exp(-2\pi i \Phi/\Phi_0) c_{\vec{i},\sigma} \quad \text{and} \quad c_{\vec{i}+L\vec{a}_y,\sigma} = c_{\vec{i},\sigma}, \qquad (3)$$

with $\Phi_0 = hc/e$ the flux quanta and L the linear length of the square lattice. The boundary conditions given by Eq. (3) account for a magnetic flux threading a torus on which the lattice is wrapped.

The interaction that we will add has the form

 © 1997 The American Physical Society

$$H_W = -W\sum_{\vec{i}} K_{\vec{i}}^2 \tag{4}$$

with positive W. The Hamiltonian

$$H = H_{tU} + H_W \tag{5}$$

has the possibility of exhibiting a quantum transition between an antiferromagnetic Mott insulating state and a superconducting $d_{x^2-y^2}$ phase. When $W=0$, the half-filled Hubbard model with a finite U is known to be a Mott insulator with long-range antiferromagnetic order. The interaction H_W can be decomposed into the following terms:

$$H_W = H_W^{(1)} + H_W^{(2)} + H_W^{(3)} + H_W^{(4)},$$

$$H_W^{(1)} = -4W\sum_{\vec{i},\sigma} c_{\vec{i},\sigma}^\dagger c_{\vec{i},\sigma} - W\sum_{\vec{i},\sigma,\vec{\delta},\vec{\delta'}} c_{\vec{i}+\vec{\delta},\sigma}^\dagger c_{\vec{i}+\vec{\delta'},\sigma},$$

$$H_W^{(2)} = -W\sum_{\vec{i},\sigma,\vec{\delta},\vec{\delta'}} (c_{\vec{i},\sigma}^\dagger c_{\vec{i},-\sigma}^\dagger c_{\vec{i}+\vec{\delta'},-\sigma} c_{\vec{i}+\vec{\delta},\sigma} + \text{H.c.}),$$

$$H_W^{(3)} = +2W\sum_{\vec{i},\vec{\delta},\vec{\delta'}} (T_{\vec{i},\delta',1}^\dagger T_{\vec{i},\delta,1} + T_{\vec{i},\delta',-1}^\dagger T_{\vec{i},\delta,-1} + T_{\vec{i},\delta',0}^\dagger T_{\vec{i},\delta,0}),$$

$$H_W^{(4)} = -2W\sum_{\vec{i},\vec{\delta},\vec{\delta'}} \Delta_{\vec{i},\delta'}^\dagger \Delta_{\vec{i},\delta}. \tag{6}$$

Here, $T_{\vec{i},\delta,1}^\dagger = c_{\vec{i},\uparrow}^\dagger c_{\vec{i}+\vec{\delta},\uparrow}^\dagger$, $T_{\vec{i},\delta,-1}^\dagger = c_{\vec{i},\downarrow}^\dagger c_{\vec{i}+\vec{\delta},\downarrow}^\dagger$, $T_{\vec{i},\delta,0}^\dagger = (c_{\vec{i},\uparrow}^\dagger c_{\vec{i}+\vec{\delta},\downarrow}^\dagger + c_{\vec{i},\downarrow}^\dagger c_{\vec{i}+\vec{\delta},\uparrow}^\dagger)/\sqrt{2}$, and $\Delta_{\vec{i},\delta}^\dagger = (c_{\vec{i},\uparrow}^\dagger c_{\vec{i}+\vec{\delta},\downarrow}^\dagger - c_{\vec{i},\downarrow}^\dagger c_{\vec{i}+\vec{\delta},\uparrow}^\dagger)/\sqrt{2}$. $H_W^{(1)}$ contains single-particle terms that renormalize the chemical potential and allow single-particle hopping between next-nearest-neighbor sites. $H_W^{(2)}$ scatters an on-site singlet to adjacent sites. In the presence of a Hubbard interaction, this term should not contribute to the low-energy physics since double occupancy is suppressed. $H_W^{(3)}$ corresponds to a triplet scattering channel. Since this term has a positive coupling constant, and triplet pairing is not favored by the Hubbard interaction, $H_W^{(3)}$ is not expected to be relevant for the low-energy physics. Finally $H_W^{(4)}$ contains the term we are interested in. The terms in $H_W^{(4)}$ with $\delta = \delta'$ contribute to the exchange interaction giving

$$2W\sum_{\vec{i},\vec{\delta}} (\vec{S}_{\vec{i}}\cdot\vec{S}_{\vec{i}+\vec{\delta}} - \tfrac{1}{4} n_{\vec{i}} n_{\vec{i}+\vec{\delta}}) \tag{7}$$

while the terms in $H_W^{(4)}$ with $\delta \neq \delta'$ contribute to a pairing interaction. Thus in the presence of the on-site Hubbard repulsion, $H_W^{(4)}$ is the relevant part of H_W in determining the low-energy properties.

As previously discussed, we have chosen the form of the interaction H_W in order to obtain a model that exhibits a transition from the antiferromagnetic Mott insulating state to a $d_{x^2-y^2}$ superconducting state and is suitable for Monte Carlo simulations. In particular integrating out the phonons from a Su-Schrieffer-Heeger type[3] term with Einstein oscillators:

$$\sum_{\vec{i},\sigma} \vec{\lambda}\cdot\vec{Q}_{\vec{i}} K_{\vec{i}} + \sum_{\vec{i}} \left(\frac{\vec{P}_{\vec{i}}^2}{2M} + \vec{Q}_{\vec{i}}^\dagger \frac{D}{2} \vec{Q}_{\vec{i}} \right), \tag{8}$$

and taking the antiadiabatic limit ($M\to 0$), generates H_W with $W = \vec{\lambda}^\dagger D^{-1}\vec{\lambda}/2$. Pairing mechanism along those lines were considered in Refs. 4 and 5. Here, however, we view this simply as a Hubbard-Stratonovitch transformation that is useful in constructing the Monte Carlo simulation.

Our general view is that the half-filled two-dimensional Hubbard model is near various instabilities. In particular, Monte Carlo calculations find a divergence in the compressibility and an unusually large dynamical exponent at the metal-insulator transition driven by the chemical potential.[6–8] In the doped state obtained with the addition of a chemical potential, the leading singlet pairing interaction is found in the $d_{x^2-y^2}$ channel.[1,9] There is clear evidence that the model is sensitive to the addition of a chemical potential. Here, we will examine the half-filled system to the interaction W.

The organization of the text is the following. In the next section, we give a description of the generalizations required to implement H_W in the projector quantum Monte Carlo (PQMC) (Refs. 10–13) and finite-temperature QMC algorithms.[14,15] In the Appendix, we discuss the construction of trial wave functions used in the PQMC. Numerical results are presented in Secs. III and IV. In Sec. III we concentrate on the charge degrees of freedom and in Sec. IV on the spin degrees of freedom. The zero-temperature data, from which we conclude the existence of a phase transition between an antiferromagnetic Mott insulating state and $d_{x^2-y^2}$ superconducting state, have already been presented in Ref. 2. At finite temperatures, we concentrate mostly on the superconducting state. We show the occurrence of a finite-temperature Kosterlitz-Thouless transition. The one-electron density of states, $N(\omega)$, the relaxation rate $1/T_1$, as well as the real and imaginary part of the spin susceptibility are calculated in the superconducting phase above and below the Kosterlitz-Thouless transition temperature. In the last section, we discuss and summarize our results.

II. QUANTUM MONTE CARLO ALGORITHMS

We have applied both the PQMC and finite-temperature QMC algorithms for numerical simulations of the Hamiltonian (5). The details of those algorithms in the case of the Hubbard model have been reviewed in the literature.[20] In this section, we discuss the generalizations required for the inclusion of the H_W term. We will concentrate on the description of the PQMC algorithm. Apart from differences in the numerical stabilization of the algorithms, the step from the PQMC to finite-temperature algorithm is straightforward and similar to the case of the Hubbard model. For the numerical simulations, it is convenient to carry out a canonical transformation, $\tilde{c}_{\vec{i},\sigma} = \exp(2\pi i\,(\Phi/\Phi_0 L)\,\vec{i}\cdot\vec{a}_x) c_{\vec{i},\sigma}$. From Eq. (3) it follows that the $\tilde{c}$ fermionic operators satisfy periodic boundary conditions. Under this canonical transformation,

$$K_{\vec{i}} = \sum_{\sigma,\vec{\delta}} (\tilde{c}_{\vec{i},\sigma}^\dagger \tilde{c}_{\vec{i}+\vec{\delta},\sigma} e^{-i\phi\vec{\delta}\cdot\vec{a}_x} + \tilde{c}_{\vec{i}+\vec{\delta},\sigma}^\dagger \tilde{c}_{\vec{i},\sigma} e^{i\phi\vec{\delta}\cdot\vec{a}_x}), \tag{9}$$

where $\phi = 2\pi(\Phi/\Phi_0 L)$. In this section we will work in this basis, and omit the *tilde* on the fermionic operators $\tilde{c}$. The inclusion of magnetic fields in QMC methods is straightforward, and has been discussed in Ref. 16.

The idea behind the PQMC algorithm is to filter out the ground state from a trial wave function $|\Psi_T\rangle$ which is required to be nonorthogonal to the ground state $|\Psi_0\rangle$,

$$\frac{\langle\Psi_0|O|\Psi_0\rangle}{\langle\Psi_0|\Psi_0\rangle} = \lim_{\Theta\to\infty} \frac{\langle\Psi_T|e^{-\Theta H}Oe^{-\Theta H}|\Psi_T\rangle}{\langle\Psi_T|e^{-2\Theta H}|\Psi_T\rangle}. \quad (10)$$

The Monte Carlo evaluation of the observable O proceeds in the following way. The first step is to carry out a Trotter decomposition of the imaginary time propagation:

$$e^{-2\Theta H} \sim (e^{-\Delta\tau H_U} e^{-\Delta\tau H_W^{(1)}} \cdots e^{-\Delta\tau H_W^{(n_w)}} e^{-\Delta\tau H_t})^m. \quad (11)$$

Here, H_t (H_U) denotes the kinetic (potential) term of the Hubbard model, $m\Delta\tau = 2\Theta$ and

$$H_W = \sum_{n=1}^{n_w} H_W^{(n)}, \quad H_W^{(n)} = -W \sum_{r=1}^{N/n_w} K_{\vec{k}(n,r)}^2$$

$$\text{and } [K_{\vec{k}(n,r)}, K_{\vec{k}(n,r')}] = 0 \forall r, r'. \quad (12)$$

The above defines the function $\vec{k}(n,r)$, $n = 1, \ldots, n_w$ and $r = 1, \ldots, N/n_w$ for an N-site lattice. Hence, $H_W^{(n)}$ is given by a sum of commuting operators. The systematic error produced by the above Trotter decomposition is of the order $\Delta\tau$. However, provided that the operators $H_W^{(n)}, H_t, H_U, O$, as well as the trial wave function $|\Psi_T\rangle$ are simultaneously real representable the prefactor of the systematic error proportional to $\Delta\tau$ in the evaluation of the observable O vanishes.[18,16] As we will see, this condition is satisfied in our calculations and the systematic error produced by the Trotter decomposition is of order $\Delta\tau^2$.

Having isolated the two-body interaction terms, one may carry out Hubbard Stratonovitch transformations so as to express the right-hand side of Eq. (11) as an imaginary time propagation of noninteracting electrons in an external field. For the Hubbard interaction, it is convenient to carry out a discrete Hubbard-Stratonovitch decomposition[19] to obtain

$$e^{-\Delta\tau H_U} = C \sum_{\vec{s}} \exp\left(\sum_{\vec{i},\vec{j},\sigma} c_{\vec{i},\sigma}^\dagger D_{\vec{i},\vec{j}}^\sigma(\vec{s}) c_{\vec{j},\sigma} \right). \quad (13)$$

Here $\vec{s}$ denotes a vector of length given by the number of sites N of HS Ising fields and

$$D_{\vec{i},\vec{j}}^\sigma(\vec{s}) = \delta_{\vec{i},\vec{j}} \cosh^{-1}(\Delta\tau U/2) s_{\vec{i}} \sigma. \quad (14)$$

The constant $C = \exp(-\Delta\tau NU/2)/2^N$ for the N-site system will be dropped below.

For the decomposition of $H_W^{(n)}$ we have used the approximate identity:

$$e^{-\Delta\tau H_W^{(n)}} = C' \sum_{\vec{l}^{(n)}} a^{(n)}(\vec{l}) \exp\left(\sum_{\vec{i},\vec{j},\sigma} c_{\vec{i},\sigma}^\dagger A_{\vec{i},\vec{j}}^{(n)}(\vec{l}) c_{\vec{j},\sigma} \right) + O(\Delta\tau^4), \quad (15)$$

where $\vec{l}^{(n)} = (l^{(n,1)}, \ldots, l^{(n,N/n_w)})$, $l^{(n,r)} = -2, -1, 1, 2$ for $r = 1, \ldots, N/n_w$, and

$$A_{\vec{i},\vec{j}}^{(n)}(\vec{l}) = \sqrt{\Delta\tau W} \sum_{r=1}^{N/n_w} \eta(l^{(n,r)}) A_{\vec{i},\vec{j}}^{(n,r)},$$

$$a^{(n)}(\vec{l}) = \prod_{r=1}^{N/n_w} \gamma(l^{(n,r)}),$$

$$A_{\vec{i},\vec{j}}^{(n,r)} = \delta_{\vec{i},\vec{k}(n,r)} (\delta_{\vec{j},\vec{i}+\vec{a}_x} e^{-i\phi} + \delta_{\vec{j},\vec{i}-\vec{a}_x} e^{i\phi} + \delta_{\vec{j},\vec{i}+\vec{a}_y} + \delta_{\vec{j},\vec{i}-\vec{a}_y}) + \delta_{\vec{j},\vec{k}(n,r)} (\delta_{\vec{i},\vec{j}+\vec{a}_x} e^{i\phi} + \delta_{\vec{i},\vec{j}-\vec{a}_x} e^{-i\phi} + \delta_{\vec{i},\vec{j}+\vec{a}_y} + \delta_{\vec{i},\vec{j}-\vec{a}_y}). \quad (16)$$

The fields η and γ take the values

$$\gamma(\pm 1) = 1 + \sqrt{6}/3, \quad \gamma(\pm 2) = 1 - \sqrt{6}/3;$$

$$\eta(\pm 1) = \pm\sqrt{2(3-\sqrt{6})}, \quad \eta(\pm 2) = \pm\sqrt{2(3+\sqrt{6})}. \quad (17)$$

The constant $C' = (1/4)^{N/n_w}$ will also be dropped below. The matrices $A^{(n,r)}$ and $A^{(n,r')}$ commute for all combinations of r and r'. The systematic error produced by the above decomposition of $H_W^{(n)}$ is of order $\Delta\tau^4$ per time slice, and hence produces an overall systematic error of order $\Delta\tau^3$. Compared to the accuracy of the Trotter decomposition (of order $\Delta\tau^2$) this is negligible.

The trial wave function is required to be given by a Slater determinant:

$$|\Psi_T\rangle = |\Psi_T^\uparrow\rangle \otimes |\Psi_T^\downarrow\rangle,$$

$$|\Psi_T^\sigma\rangle = \prod_{n=1}^{N_p^\sigma} \left(\sum_{\vec{i}} c_{\vec{i},\sigma}^\dagger P_{\vec{i},n}^\sigma \right) |0^\sigma\rangle. \quad (18)$$

Here N_p^σ denotes the number of particles in a given spin sector, $|0^\sigma\rangle$ is the vacuum in the spin-σ sector, and P^σ is an $N \times N_p^\sigma$ rectangular matrix where N is the number of sites.

One may now integrate the fermionic degrees of freedom and define a probability distribution:

$$\Pr(\vec{s},\vec{l}) = \frac{a(\vec{l}) \det(M^\uparrow(\vec{l},\vec{s})) \det(M^\downarrow(\vec{l},\vec{s}))}{\sum_{\vec{s},\vec{l}} a(\vec{l}) \det(M^\uparrow(\vec{l},\vec{s})) \det(M^\downarrow(\vec{l},\vec{s}))}. \quad (19)$$

The fields $\vec{s}$, $\vec{l}$ acquire an additional time index $\tau: 1, \ldots, m$, $a(\vec{l}) = \Pi_{r,n,\tau} \gamma(l_\tau^{(n,r)})$ and

$$M^\sigma(\vec{l},\vec{s}) = P^{\dagger,\sigma} B_{\vec{s},\vec{l}}^\sigma(2\Theta,0) P^\sigma,$$

$$B_{\vec{s},\vec{l}}(\Theta_2,\Theta_1) = \prod_{\tau=\tau_1+1}^{\tau_2} e^{D_\tau^\sigma(\vec{s})} e^{A_\tau^{(1)}(\vec{l})} \cdots e^{A_\tau^{(n_w)}(\vec{l})} e^{-\Delta\tau T}. \quad (20)$$

Here, $\Theta_1 = \tau_1\Delta\tau$, $\Theta_2 = \tau_2\Delta\tau$, and $H_t = \Sigma_{\vec{i},\vec{j},\sigma} c_{\vec{i},\sigma}^\dagger T_{\vec{i},\vec{j}} c_{\vec{j},\sigma}$ corresponds to the kinetic energy of the Hubbard model. Observables may now be evaluated by

$$\frac{\langle\Psi_T|e^{-\Theta H}Oe^{-\Theta H}|\Psi_T\rangle}{\langle\Psi_T|e^{-2\Theta H}|\Psi_T\rangle}=\sum_{\vec{s},\vec{l}}\ \Pr(\vec{s},\vec{l})\langle O\rangle_{\vec{s},\vec{l}}+O(\Delta\tau^2). \tag{21}$$

For a given set of fields $\vec{s},\vec{l}$, Wicks theorem applies and it suffices to calculate single-particle Green functions. They are given by

$$\langle c_{\vec{i},\sigma}c^{\dagger}_{\vec{j},\sigma'}\rangle_{\vec{s},\vec{l}}=\delta_{\sigma,\sigma'}(I-B^{\sigma}_{\vec{s},\vec{l}}(\Theta,0)P^{\sigma}M^{\sigma}(\vec{s},\vec{l})^{-1}\times P^{\dagger,\sigma}B^{\sigma}_{\vec{s},\vec{l}}(2\Theta,\Theta))_{\vec{i},\vec{j}}. \tag{22}$$

Here I is the unit matrix, $I_{\vec{i},\vec{j}}=\delta_{\vec{i},\vec{j}}$.

As mentioned previously, the Monte Carlo simulation, for the half-filled case, does not suffer from the sign problem. That $\Pr(\vec{s},\vec{l})$ is positive for all values of the fields $\vec{s}$ and $\vec{l}$ follows by carrying out a particle-hole transformation in say the up spin sector: $c^{\dagger}_{\vec{i},\uparrow}=(-1)^{i_x+i_y}h_{\vec{i},\uparrow}$. Since the electron vacuum $|0^{\uparrow}\rangle$ is given by $|0^{\uparrow}\rangle=\Pi_{\vec{i}}h^{\dagger}_{\vec{i},\uparrow}|0^{h,\uparrow}\rangle$ one has

$$|\Psi^{\uparrow}_T\rangle=\prod_{n=1}^{N^{\uparrow}_p}\left(\sum_{\vec{i}}\ h_{\vec{i},\uparrow}(-1)^{i_x+i_y}P^{\uparrow}_{\vec{i},n}\right)\prod_{\vec{i}}\ h^{\dagger}_{\vec{i},\uparrow}|0^{h,\uparrow}\rangle$$

$$\equiv\prod_{n=1}^{N-N^{\uparrow}_p}\left(\sum_{\vec{i}}\ h^{\dagger}_{\vec{i},\uparrow}\tilde{\bar{P}}_{\vec{i},n}\right)|0^{h,\uparrow}\rangle. \tag{23}$$

The above equation defines $\widetilde{P}$ and $\tilde{\bar{P}}_{\vec{i},n}$ denotes the complex conjugate of $\widetilde{P}_{\vec{i},n}$. Under the above transformation, one has

$$\det(M^{\uparrow}_{\vec{s},\vec{l}})=e^{\alpha\Sigma_{\vec{i},\tau}s_{\vec{i},\tau}}\overline{\det(\widetilde{P}^{\dagger}B^{\downarrow}_{\vec{s},\vec{l}}(2\Theta,0)\widetilde{P})}, \tag{24}$$

where $\alpha=\cosh^{-1}(\Delta\tau U/2)$. The complex conjugation comes from the fact that if electrons feel a flux Φ, holes are submitted to a flux $-\Phi$. The complex conjugation changes the sign of the flux Φ. Provided that the particle number in given spin sectors satisfy $N-N^{\uparrow}_p=N^{\downarrow}_p$ and that the trial wave function satisfies $\widetilde{P}=P^{\downarrow}$ one has

$$\det(M^{\uparrow}_{\vec{s},\vec{l}})=e^{\alpha\Sigma_{\vec{i},\tau}s_{\vec{i},\tau}}\overline{\det(M^{\downarrow}_{\vec{s},\vec{l}})}, \tag{25}$$

from which the positivity of the probability distribution $\Pr(\vec{s},\vec{l})$ follows. We have used a trial wave function that satisfies the above condition for the positivity of the probability distribution. We furthermore require $|\Psi_T\rangle$ to be a spin singlet:

$$\sum_{\vec{i},\vec{j}}\ \vec{S}_{\vec{i}}\cdot\vec{S}_{\vec{j}}|\Psi_T\rangle=0, \tag{26}$$

where $\vec{S}_{\vec{i}}$ is the spin operator on site $\vec{i}$. An explicit construction of trial wave functions showing no sign problem, being spin singlets and if necessary real representable in real space is given in the Appendix.

The sum over the Hubbard-Stratonovitch fields is carried out with Monte Carlo methods. One sweeps sequentially through the space-time lattice and proposes single spin-flip updates. The ratio of new-to-old probabilities under a local change $l^{(n,r)}_{\tau}\rightarrow l'^{(n,r)}_{\tau}$ is best calculated in a basis where the matrix $A^{(n,r)}_{\vec{i},\vec{j}}$ is diagonal. Since in this basis $A^{(n,r)}_{\vec{i},\vec{j}}$ has only two nonvanishing eigenvalues, the ratio of probabilities involves the knowledge of four Green functions per spin sector. Note that under a proposed local move $s_{\vec{i},\tau}\rightarrow s'_{\vec{i},\tau}$ the ratio of probabilities is given by a single Green function per spin sector. In case of acceptance of the spin flip, the required updating is two times more expensive in the case of an $l^{(n,r)}_{\tau}\rightarrow l'^{(n,r)}_{\tau}$ move than for an $s_{\vec{i},\tau}\rightarrow s'_{\vec{i},\tau}$ move. The numerical stabilization of the algorithm is identical to that used for Hubbard calculations. This concludes our description of the PQMC algorithm.

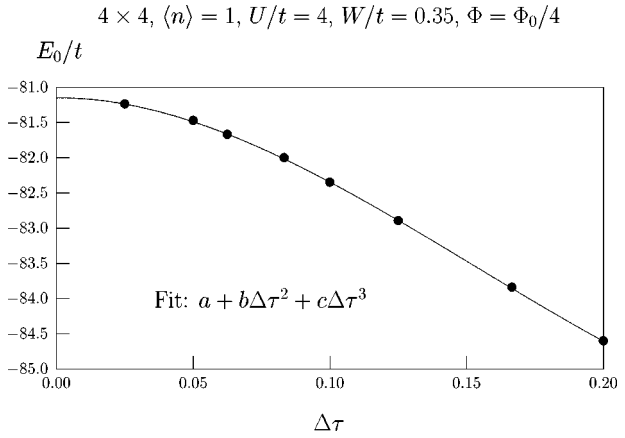

FIG. 1. Total energy as obtained with the PQMC at $\Theta t=1$ as a function of $\Delta\tau$. The solid line is a least square fit to the form $a+b\Delta\tau^2+c\Delta\tau^3$ with $a=-81.146\pm0.015$, $b=-153\pm3$, and $c=334\pm15$. The energy unit is set by $t=1$.

The finite-temperature QMC algorithm is a grand canonical simulation that evaluates

$$\langle O\rangle=\frac{\mathrm{Tr}(e^{-\beta H}O)}{\mathrm{Tr}(e^{-\beta H})}, \tag{27}$$

where the trace runs over the Fock space and β denotes the inverse temperature. The finite-temperature QMC algorithm is conceptually similar to that of the PQMC.[20] Both the PQMC (Ref. 17) and finite-temperature QMC algorithms may be used to calculate imaginary time displaced correlation functions. The dynamical results presented here stem from the use of the classic maximum entropy method[21,22] to analytically continue imaginary time data produced by the finite-temperature QMC algorithm.

We are now in a position to test and compare the PQMC and finite-temperature algorithms. As mentioned previously, the systematic error produced by the Trotter decomposition is of the order $\Delta\tau^2$ provided that the operators $H^{(n)}_W, H_t, H_U, O$, as well as the trial wave function $|\Psi_T\rangle$ are simultaneously real representable. This may be checked explicitly by calculating the energy with the PQMC algorithm at $\Phi/\Phi_0=0.25$, $U/t=4$, $W/t=0.35$ on a 4×4 lattice with $2\Theta t=1$ for various values of $\Delta\tau$. The results are plotted in Fig. 1. They follow well an $a+b\Delta\tau^2+c\Delta\tau^3$ form. Note that the $\Delta\tau^3$ term, originates from the approximate Hubbard-Stratonovitch decomposition of H_W. We have carried out most of our PQMC simulations at $\Delta\tau=0.0625t$, which is sufficiently small for our purposes.

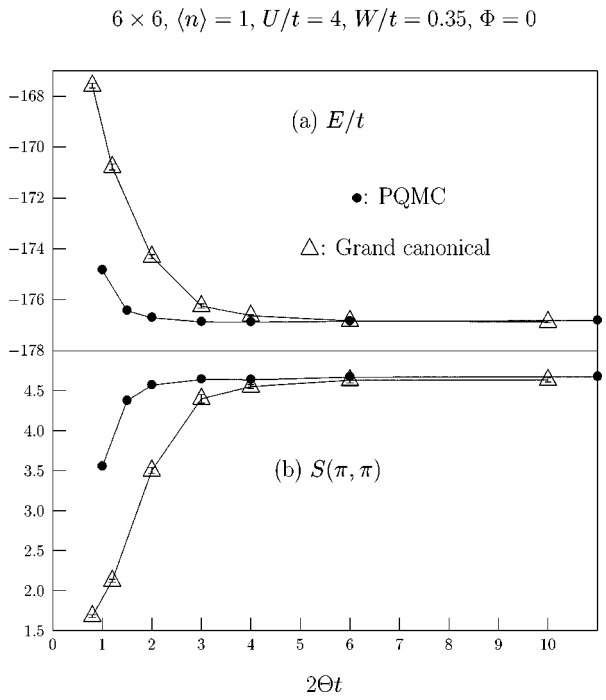

FIG. 2. (a) Total energy E and (b) spin structure factor at $\vec{Q}=(\pi,\pi)$ as obtained from the finite temperature QMC algorithm at $\beta=2\theta$ and from the PQMC algorithm.

Figure 2 shows plots of the total energy E as well as the spin structure factor at $\vec{Q}=(\pi,\pi)$, $S(\vec{Q})=\frac{4}{3}\Sigma_{\vec{r}}e^{i\vec{Q}\vec{r}}\langle\vec{S}_{\vec{r}}\vec{S}_{\vec{0}}\rangle$ as obtained with the PQMC and finite-temperature algorithms. For the finite-temperature data, we set $\beta=2\Theta$ and measure the observables with Eq. (27). The same observables are evaluated with Eq. (21) and the above-described trial wave function. We set $\Delta\tau=0.1$ and in the case of the PQMC algorithm measure observables on the ten central time slices. For observables that do not commute with the Hamiltonian, this yields an effective projection parameter $\Theta^{\text{eff}}=\Theta-0.5t$. We consider a 6×6 lattice at $U/t=4$, $W/t=0.35$, and $\Phi=0$. The trial wave function used here is constructed as shown in Eq. (A4) and the orthogonal transformation used is obtained by diagonalizing the Hamiltonian of Eq. (A6) at a numerically infinitesimal value of δ. We have used this trial wave function for all our calculations at $\Phi=0$. In the limit of large Θt, both the finite-temperature and PQMC results converge to the same value within the error bars. We observe that ground-state properties are obtained more efficiently within the PQMC approach.

III. CHARGE DEGREES OF FREEDOM

In this section, we consider the charge degrees of freedom at zero and finite temperatures. We start by showing that at zero temperature, half-band filling, and constant value of the Hubbard repulsion, $U/t=4$, W/t triggers a transition between an insulator and a $d_{x^2-y^2}$ superconductor. The transition is found to occur at $W_c/t\sim0.3$. We then consider the superconducting state at $W/t=0.35$ and give numerical evidence for the occurrence of a finite-temperature Kosterlitz-Thouless transition. The temperature dependence of the one-electron density of states, $N(\omega)$, is analyzed.

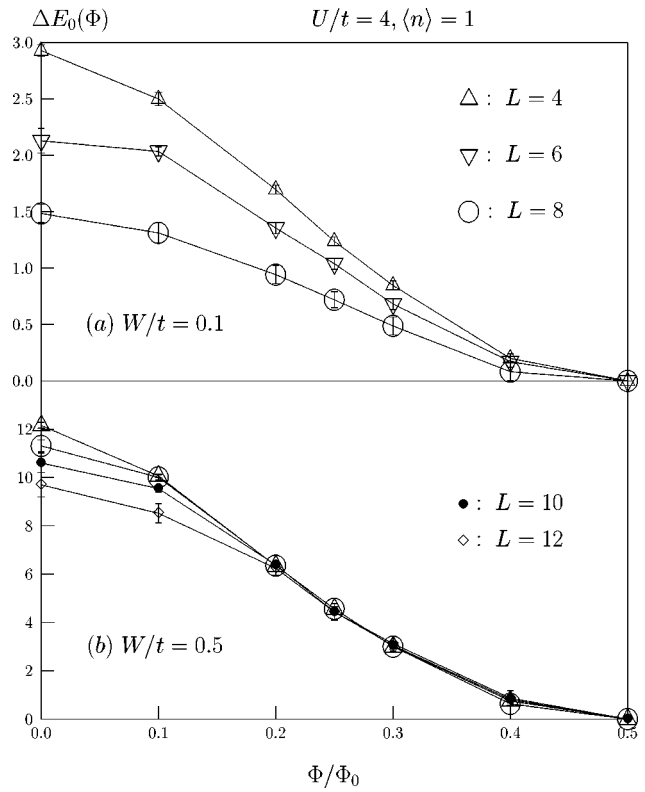

FIG. 3. $\Delta E_0(\Phi)\equiv E_0(\Phi)-E_0(\Phi_0/2)$ at (a) $W/t=0.1$ and (b) $W/t=0.5$

A. Zero temperature

An efficient and general method to distinguish between an insulator and superconductor is to compute the ground-state energy as a function of a twist Φ in the boundary condition along one lattice direction: $E_0(\Phi)$. In the case of an insulator, the wave function is localized and hence, an exponential decay of $\Delta E_0(\Phi)\equiv E_0(\Phi)-E_0(\Phi_0/2)$ as a function of lattice size is expected.[23] In the spin density wave (SDW) approximation for the half-filled Hubbard model, one obtains $\Delta E_0(\Phi)=\alpha(\Phi)L\exp(-L/\xi)$, where ξ is the localization length of the wave function. On the other hand, for a superconductor [i.e., off-diagonal long-range order (ODLRO)], $\Delta E_0(\Phi)$ shows anomalous flux quantization: $\Delta E_0(\Phi)$ is a periodic function of Φ with period $\Phi_0/2$ and a nonvanishing energy barrier is to be found between the flux minima[24–26,16] so that $\Delta E_0(\Phi_0/4)$ remains finite as $L\to\infty$. In general, this functional form of $\Delta E_0(\Phi)$ should occur only in the thermodynamic limit.

Figure 3 shows $\Delta E_0(\Phi)$ at $W/t=0.1$ and $W/t=0.5$. At $W/t=0.1$, and as expected for an insulator, $\Delta E_0(\Phi)$ is suppressed with growing lattice sizes for all values of Φ. In contrast, at $W/t=0.5$ one notes that for values of $1/4<\Phi/\Phi_0<1/2$, $\Delta E_0(\Phi_0)$ is very stable against growing lattice sizes. On the other hand, at $\Phi=0$, $\Delta E_0(\Phi)$ decreases with growing lattice sizes. We interpret the data as a finite-size indication of anomalous flux quantization. At the end of Sec. IV A we will argue that this *slow* size scaling of $\Delta E_0(\Phi)$ in the vicinity of $\Phi=0$ is related to the nature of the spin degrees of freedom in the superconducting state. Very similar results were obtained in the case of the repulsive and attractive Hubbard models at half-filling.[26,16]

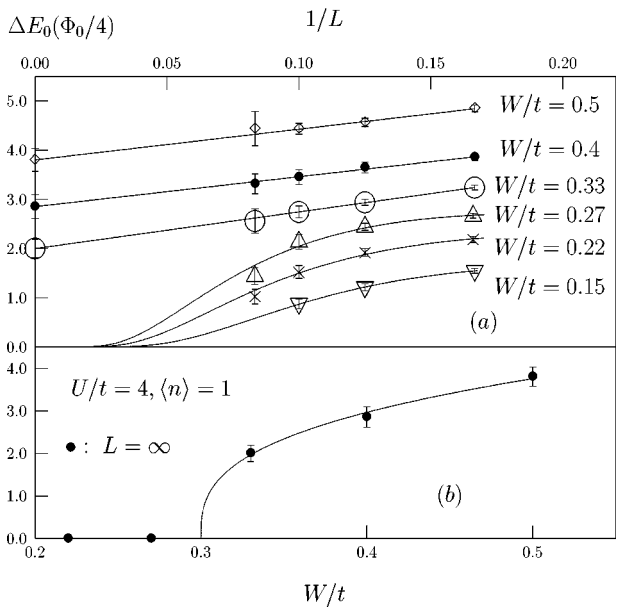

FIG. 4. (a) $\Delta E_0(\Phi_0/4) \equiv E_0(\Phi_0/4) - E_0(\Phi_0/2)$ vs $1/L$ for several values of W/t. For $W/t < 0.3$ the solid lines correspond to a least-square fit of the data to the SDW form: $L \exp(-L/\xi)$. For $W/t > 0.3$ the QMC data are compatible with a $1/L$ scaling to a finite constant. The solid lines are least-square fit to this form. (b) Extrapolated value of $\Delta E_0(\Phi_0/4)$ vs W/t. The solid line is a guide to the eye.

To best distinguish between the insulating and superconducting states, we consider the size scaling of the quantity $\Delta E_0(\Phi_0/4)$ for various values of W/t as in Fig. 4(a). One observes a change in the size scaling of $\Delta E_0(\Phi_0/4)$ as W/t decreases from $W/t = 0.5$ to $W/t = 0.22$. From these measurements, we estimate that the change occurs in the vicinity of $W/t = 0.3$. For values of $W/t < 0.3$, $\Delta E_0(\Phi_0/4)$ is consistent with the SDW form whereas for $W/t \geqslant 0.33 \Delta E_0(\Phi_0/4)$ may be extrapolated to a finite value with finite-size corrections proportional to $1/L$. The extrapolated value of $\Delta E_0(\Phi_0/4)$ versus W/t is plotted in Fig. 4(b) and the quantum transition between a Mott insulator and superconductor occurs at $W/t \sim 0.3$.

In order to determine the symmetry of the superconducting order parameter we have computed in Ref. 2 equal time pair-field correlations in the extended s-wave and $d_{x^2-y^2}$ channels:

$$P_{d,s}(\vec{r}) = \langle \Delta^{\dagger}_{d,s}(\vec{r}) \Delta_{d,s}(\vec{0}) \rangle \tag{28}$$

with

$$\Delta^{\dagger}_{d,s}(\vec{r}) = \sum_{\sigma,\vec{\delta}} f_{d,s}(\vec{\delta}) \sigma c^{\dagger}_{\vec{r},\sigma} c^{\dagger}_{\vec{r}+\vec{\delta},-\sigma}. \tag{29}$$

Here, $f_s(\vec{\delta}) = 1$ and $f_d(\vec{\delta}) = 1(-1)$ for $\vec{\delta} = \pm \vec{a_x}(\pm \vec{a_y})$. On our largest lattice size, $L = 16$, and in the superconducting state at $W/t = 0.6$ the dominant signal at $\vec{r} = (L/2, L/2)$ is obtained in the d-wave channel.[2] Another evidence of $d_{x^2-y^2}$ superconductivity is seen in the single-particle occupation number $n(\vec{k})$. At $W/t = 0.6$ and on sizes up to $L = 16$, the QMC data are consistent with the mean-field equation:

$$n(\vec{k}) = 1 - \frac{\epsilon_{\vec{k}}}{\sqrt{\Delta^2_{\vec{k}} + \epsilon^2_{\vec{k}}}}. \tag{30}$$

Here $\epsilon_{\vec{k}}$ corresponds to the single-particle dispersion relation and $\Delta_{\vec{k}} = (\Delta_0/2)[\cos(k_x) - \cos(k_y)]$.[2] In the next section, we will give further evidence that the superconducting state has $d_{x^2-y^2}$ symmetry.

B. Finite temperature: $W/t = 0.35$

For values of $W/t > W_c/t \sim 0.3$, one expects the occurrence of a finite-temperature Kosterlitz-Thouless transition. To detect this transition we consider the quantity

$$\Delta E(\Phi, T) = E(\Phi, T) - E(\Phi = \Phi_0/2, T). \tag{31}$$

In the framework of a Kosterlitz-Thouless[27,28] transition one expects in the thermodynamic limit

$$\Delta E(\Phi_0/4, T) \sim \delta(T - T_{\mathrm{KT}}), \tag{32}$$

where T_{KT} is the Kosterlitz-Thouless transition temperature. The above follows by considering the free energy $F(\Phi) = -1/\beta \ln \mathrm{Tr} e^{-\beta H(\Phi)}$. Expanding F around $\Phi = \Phi_0/2$ yields

$$F(\Phi) = F(\Phi_0/2) + \frac{1}{2}\left(\frac{\Phi - \Phi_0/2}{\Phi_0}\right)^2 D_s(\beta) + O\left(\left(\frac{\Phi - \Phi_0/2}{\Phi_0}\right)^4\right)$$

where

$$D_s(\beta) = -\left(\frac{2\pi}{L}\right)^2 \left(\langle \widetilde{K}_x \rangle + \int_0^{\beta} d\tau \langle J_x(\tau) J_x(0) \rangle \right),$$

$$J_x = \sum_{\vec{i}} t j^x_{\vec{i}} + W\{K_{\vec{i}} + K_{\vec{i}+\vec{a}_x}, j^x_{\vec{i}}\},$$

$$\widetilde{K}_x = \sum_{\vec{i}} t k^x_{\vec{i}} - 2W(j^x_{\vec{i}} + j^x_{\vec{i}-\vec{a}_x})^2 + W\{K_{\vec{i}} + K_{\vec{i}+\vec{a}_x}, k^x_{\vec{i}}\},$$

$$j^x_{\vec{i}} = -i \sum_{\sigma} (c^{\dagger}_{\vec{i},\sigma} c_{\vec{i}+\vec{a}_x,\sigma} - c^{\dagger}_{\vec{i}+\vec{a}_x,\sigma} c_{\vec{i},\sigma}),$$

and

$$k^x_{\vec{i}} = -\sum_{\sigma} (c^{\dagger}_{\vec{i},\sigma} c_{\vec{i}+\vec{a}_x,\sigma} + c^{\dagger}_{\vec{i}+\vec{a}_x,\sigma} c_{\vec{i},\sigma}). \tag{33}$$

The boundary conditions for the calculation of the superfluid density D_s satisfies $c_{\vec{i}+L\vec{a}_x,\sigma} = -c_{\vec{i},\sigma}$ and $c_{\vec{i}+L\vec{a}_y,\sigma} = c_{\vec{i},\sigma}$. Hence,

$$\Delta E(\Phi, T) = \frac{\partial}{\partial \beta}(\beta F(\Phi) - \beta F(\Phi_0/2)) \sim \frac{1}{2}\left(\frac{\Phi - \Phi_0/2}{\Phi_0}\right)^2 \left(D_s - T \frac{\partial}{\partial T} D_s \right). \tag{34}$$

At T_{KT}, D_s is expected to show a universal jump[28] so that $(\partial/\partial T) D_s$ behaves like a Dirac δ function and Eq. (32) follows. Such signatures of the Kosterlitz-Thouless transition have already been observed in classical[29] and quantum XY models[30] as well as in the attractive Hubbard model.[31,16]

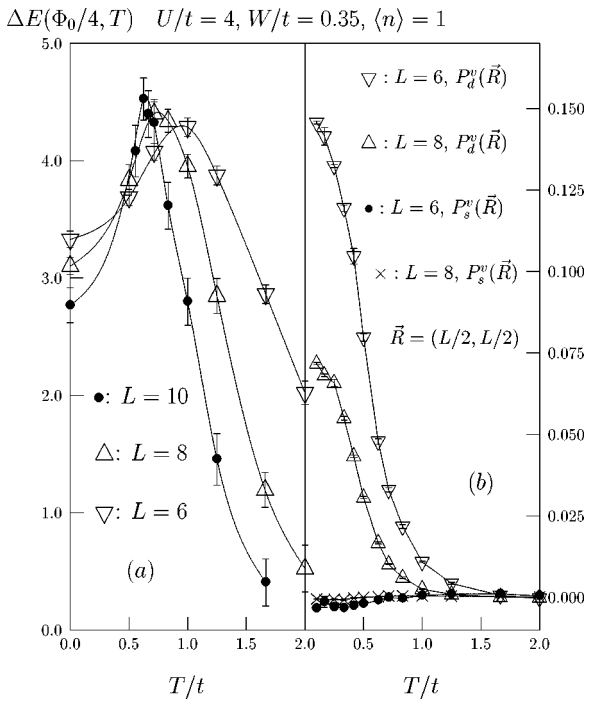

FIG. 5. (a) $\Delta E(\Phi_0/4,T)$ as defined in Eq. (31). (b) Vertex contribution of the equal time pair-field correlations as defined in Eq. (36). Here we use periodic boundary conditions in both lattice directions [i.e., $\Phi=0$ in Eq. (3)].

Figure 5(a) plots $\Delta E(\Phi_0/4,T)$ at $W/t=0.35$ and $U/t=4$ for lattice sizes ranging from $L=6$ to $L=10$. For each considered lattice size, $\Delta E(\Phi_0/4,T)$ shows a maximum at finite temperature. For a given lattice size, we define T_{KT} by this maximum and obtain $T_{\mathrm{KT}}\sim 0.95$, 0.75, 0.65 for the lattice sizes $L=6$, 8, 10, respectively. We note that the scaling of the peak height is influenced by the size dependence of T_{KT} due to the linear T term in front of $(\partial/\partial T)\,D_s$ [see Eq. (34)]. The extrapolation of T_{KT} to the thermodynamic limit is hard. However, we recall that the size scaling of the zero-temperature energy difference $\Delta E_0(\Phi_0/4)$ followed well $a+b/L$ form. Since $\Delta E_0(\Phi_0/4)$ is proportional to the zero-temperature superfluid density, it is plausible to assume that the size dependence of T_{KT} equally follows an $a+b/L$ form. The above three finite-size values of T_{KT} are consistent with this ansatz, and we obtain

$$T_{\mathrm{KT}}\sim 0.2t+4.5t/L \quad \text{at} \quad W/t=0.35. \tag{35}$$

Figure 5(b) plots the vertex contribution to the equal-time pair-field correlations[32] both in the s and $d_{x^2-y^2}$ channels for the $L=6$ and $L=8$ lattices at the largest distance: $\vec{R}=(L/2,L/2)$. This quantity is given by

$$P_{d,s}^v(\vec{r})=P_{d,s}(\vec{r})-\sum_{\sigma,\vec{\delta},\vec{\delta}'} f_{d,s}(\vec{\delta})f_{d,s}(\vec{\delta}')(\langle c^\dagger_{\vec{r},\sigma}c_{\vec{\delta}',\sigma}\rangle \times\langle c^\dagger_{\vec{r}+\vec{\delta},-\sigma}c_{\vec{0},-\sigma}\rangle+\langle c^\dagger_{\vec{r},\sigma}c_{\vec{0},\sigma}\rangle\langle c^\dagger_{\vec{r}+\vec{\delta},-\sigma}c_{\vec{\delta}',-\sigma}\rangle). \tag{36}$$

Per definition, $P_{d,s}^v(\vec{r})\equiv 0$ in the absence of interactions. An enhancement of the d-wave signal at an energy scale set by T_{KT} is observed. In contrast, the s-wave response vanishes for all considered temperatures. Contrary to the $\Delta E(\Phi_0/4,T)$ data, those calculations were carried out at $\Phi=0$.

We now consider the one-electron density of states: $N(\omega)=(1/N)\,\Sigma_{\vec{k}}A(\vec{k},\omega)$ with

$$G(\vec{k},\tau)=\frac{1}{\pi}\int_{-\infty}^{\infty}d\omega\,\frac{e^{-\tau\omega}}{1+e^{-\beta\omega}}A(\vec{k},\omega), \tag{37}$$

where $G(\vec{k},\tau)=\Sigma_\sigma\langle c_{\vec{k},\sigma}(\tau)c^\dagger_{\vec{k},\sigma}\rangle$, $\tau>0$, and $c_{\vec{k},\sigma}(\tau)=e^{\tau H}c_{\vec{k},\sigma}e^{-\tau H}$. We have used the classic maximum entropy method to obtain dynamical data from imaginary time Green functions. We chose a flat default model for $N(\omega)$ and enforced the following sum rules:

$$\int_{-\infty}^{\infty}d\omega N(\omega)=2\pi,$$

$$\int_{-\infty}^{\infty}d\omega N(\omega)\omega\,\tanh(\beta\omega/2)=\frac{\pi}{N}\sum_{\vec{k},\sigma}\langle[c^\dagger_{\vec{k},\sigma},[H,c_{\vec{k},\sigma}]]\rangle. \tag{38}$$

The calculations were carried out at $\Phi=\Phi_0/2$. The data at temperatures lesser and greater than T_{KT} are plotted in Fig. 6. We consider 6×6 to 10×10 lattices. For all three considered lattices sizes, one sees the onset of a pseudogap in the temperature range of T_{KT}. At *lower* temperatures than shown in Fig. 6, $N(\omega)$ suffers form size effects. The onset of finite-size effects on small lattices (i.e., $L=6$ and $L=8$) coincides approximately with the magnetic scale $J\sim 0.5t$, which will be determined in the next section. As the lattice size increases, one can go below the J scale without noticing an anomaly in $N(\omega)$. This may be seen explicitly in Fig. 6(m) where $T=0.33t<J$. We may estimate the value of the superconducting gap Δ_{sc} by the peak position in $N(\omega)$, at the lowest-temperature scale presented in Fig. 6. For the three considered lattice sizes, the data are consistent with $\Delta_{\mathrm{sc}}/T_{\mathrm{KT}}\sim 2.5$. The peak position decreases as a function of decreasing temperature. On the 10×10 lattice, we have looked more systematically at temperatures above T_{KT}. The data show a pseudogap feature above T_{KT}. It is not clear if this aspect of the data will survive in the thermodynamic limit.

IV. SPIN DEGREES OF FREEDOM

As in the previous section, we first concentrate on the zero-temperature spin correlations and show that the long-range antiferromagnetic order disappears at $W_c/t\sim 0.3$. We then study finite-temperature spin dynamics in the superconducting phase at $W/t=0.35$.

A. Zero temperature

To detect the existence of long-range magnetic order, we compute the real-space spin-spin correlations:

$$S(\vec{r})=\tfrac{4}{3}\langle\vec{S}(\vec{r})\vec{S}(\vec{0})\rangle, \tag{39}$$

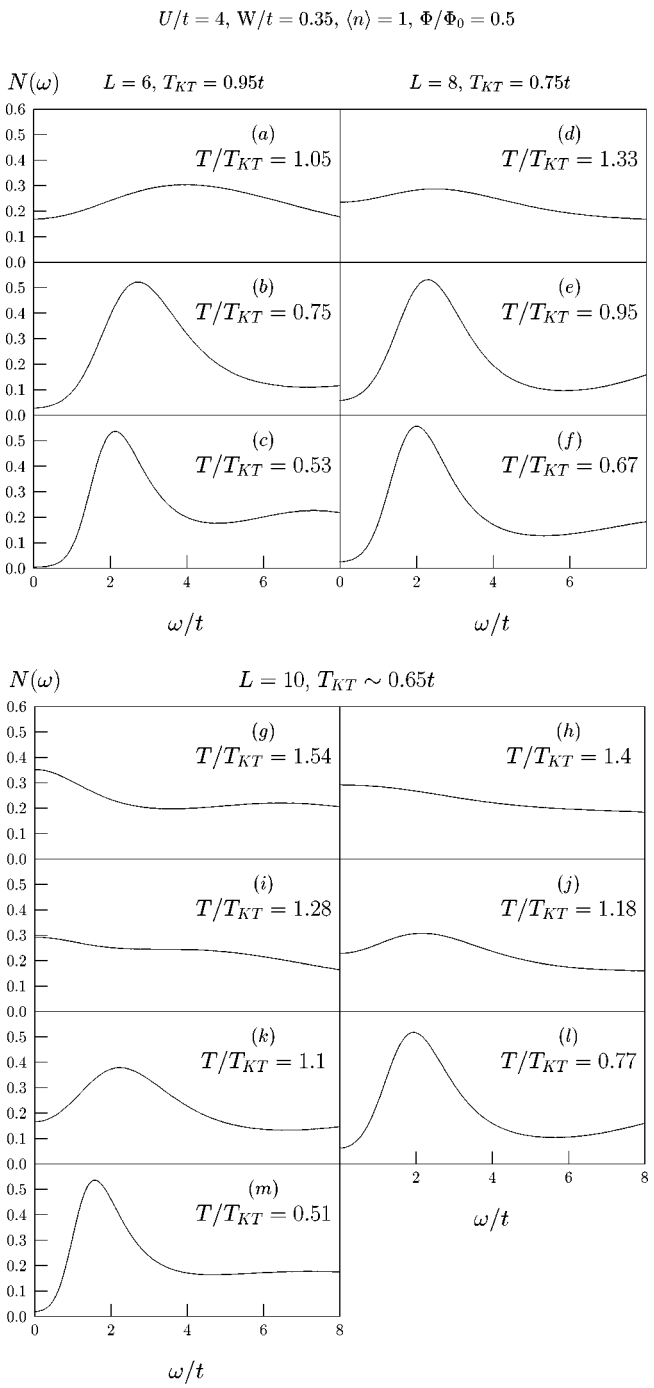

FIG. 6. One-electron density of states as a function of temperature and lattice size in the superconducting state at $W/t=0.35$ and $U/t=4$. $L=6$: (a)–(c). $L=8$: (d)–(f). $L=10$: (g)–(m).

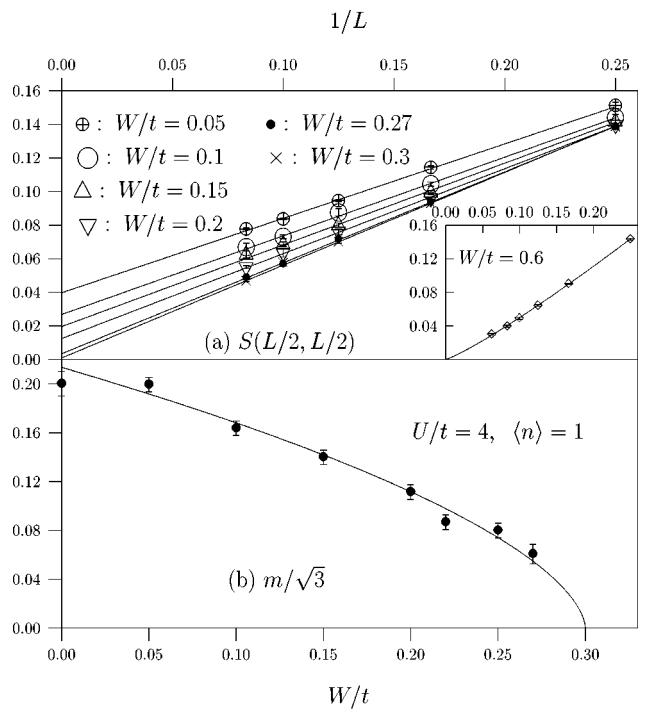

FIG. 7. (a) $S(L/2,L/2)$ vs $1/L$ for several values of W/t. The solid lines correspond to least-square fits of the QMC data to the form $1/L$. Inset: $S(L/2,L/2)$ vs $1/L$ at $W/t=0.6$. The solid is a least-square fit to the form $L^{-\alpha}$. (b) Staggered moment as obtained from (a) vs W/t. The data point at $W/t=0$ is taken from Ref. 15. At $W/t=0.3$, we were unable to distinguish m from zero within our statistical uncertainty. The solid line is a guide to the eye. The calculations in this figure were carried out at $\Phi=0$ [see Eq. (3)].

where $\vec{S}(\vec{r})$ denotes the spin operator on site $\vec{r}$. For values of $W/t<0.3$ and lattice sizes ranging from $L=4$ to $L=12$, $S(L/2,L/2)$, may be fitted to a $1/L$ form and scales to a finite value, as shown in Fig. 7(a). We therefore conclude that long-range antiferromagnetic order is present for $W/t<0.3$. The associated staggered moment, $m=\lim_{L\to\infty}\sqrt{3S(L/2,L/2)}$, is plotted in Fig. 7(b). The data are consistent with a continuous decay of m as W/t increases towards 0.3. At $W/t=0.3$, we were unable to distinguish m from zero within our statistical uncertainty. Hence, we conclude that long-range antiferromagnetic order vanishes at $W/t\sim 0.3$. Therefore, within our numerical resolution, the antiferromagnetic transition point is not separated from the superconductor-insulator transition point. Well within the $d_{x^2-y^2}$ superconducting phase the spin-spin correlations remain sizable. In fact, at $W/t=0.6$, lattice sizes ranging from $L=4$ to $L=16$, $S(L/2,L/2)$ scales as $L^{-\alpha}$ with $\alpha=1.16\pm0.01$ as shown in the inset of Fig. 7(a). This power-law decay of the spin-spin correlations in the superconducting state arise because of the nodes in the $d_{x^2-y^2}$ gap. Following Ref. 33 one can approximate the spin susceptibility, $\chi(\vec{q},i\omega_m)$, in the superconducting state by inserting the irreducible BCS spin susceptibility, $\chi_0^{\rm BCS}(\vec{q},i\omega_m)$, in the random-phase approximation (RPA) form of $\chi(\vec{q},i\omega_m)$: $\chi_{\rm RPA}(\vec{q},i\omega_m)=\chi_0^{\rm BCS}(\vec{q},i\omega_m)/[1-U\chi_0^{\rm BCS}(\vec{q},i\omega_m)]$. Here, ω_m corresponds to Matsubara frequencies. Within this approximation and at half-band filling, the spin-spin correlations for a $d_{x^2-y^2}$ superconducting order parameter show a power-law decay: $S^{\rm RPA}(L/2,L/2)\sim L^{-3.5}$. In contrast, the spin-spin correlations in an s-wave superconductor decay exponentially. Thus, the fact that spin-spin correlations remain critical in the superconducting state, may be attributed to the node and phase factors of the $d_{x^2-y^2}$ superconducting gap.

The very slow decay of the spin-spin correlations in the superconducting state revealed by the QMC data shows the extreme compatibility between a $d_{x^2-y^2}$ superconductor and substantial short-range antiferromagnetic spin-spin correla-

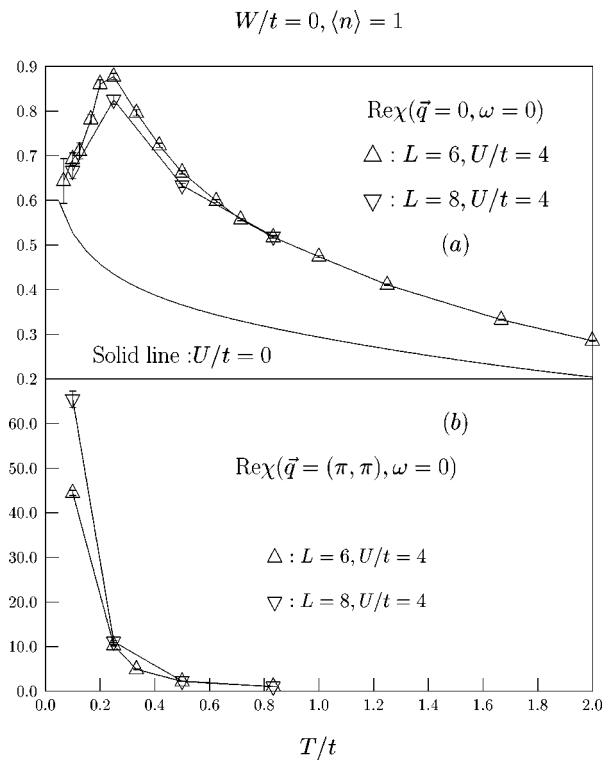

FIG. 8. (a) Uniform (b) staggered static spin susceptibility for the Hubbard model (i.e., $W/t=0$) at $U/t=4$. The solid line with no symbols in (a) corresponds to $\chi(\vec{q}=0,\omega=0)$ at $U=W=0$. The calculations were carried out at $\Phi=0$ [see Eq. (3)].

tions. In the superconducting state, the spin stiffness vanishes since spin-spin correlations decay more rapidly than $\cos(\vec{Q}\vec{r})/|\vec{r}|$, where $\vec{Q}=(\pi,\pi)$. However, since $S(\vec{r})$ decays slower than $\cos(\vec{Q}\vec{r})/|\vec{r}|^2$ and the dimension is equal to two, $S(\vec{Q})\sim\Sigma_{\vec{r}} e^{i\vec{Q}\vec{r}}S(\vec{r})$ diverges.

At this point, we can offer an explanation of why it is convenient to study charge degrees of freedom at $\Phi/\Phi_0=0.5$ and spin degrees of freedom at $\Phi=0$. We have just mentioned that, in the superconducting state, the spin-spin correlations decay as $1/|\vec{r}|^{\alpha}$ where α is slightly larger than one ($\alpha\sim 1.16$ at $W/t=0.6$). On a finite lattice, it is hard to distinguish between true long-range order and this slow decay. Choosing antiperiodic boundary conditions in one lattice direction and periodic boundary condition in the other (i.e., $\Phi/\Phi_0=0.5$), renders the ground state of the half-filled noninteracting system ($U=W=0$) nondegenerate. In a weak-coupling approach, one may understand that this choice of boundary conditions introduces frustration in antiferromagnetic correlations since on a finite lattice $\chi_0(\vec{Q},\omega=0)$ takes a finite value in the zero-temperature limit. In contrast, and on a finite lattice with periodic boundary conditions (i.e., $\Phi=0$) $\chi_0(\vec{Q},\omega=0)$ diverges in the zero-temperature limit. Here, χ_0 denotes the spin susceptibility at $U=W=0$. This frustration of the spin degrees of freedom introduced by the boundary condition minimizes the size dependence of charge degrees of freedom. This *pathology* may be seen explicitly in Fig. 3(b) where the superfluid density should, in principle, be given by the curvature of $\Delta E_0(\Phi)$ at $\Phi=0$ or $\Phi=\Phi_0/2$. At $\Phi=0$, the size scaling of this quantity is hard to extract from simulations up to $L=12$.

B. Finite temperature: $W/t=0.35$

We first consider the static spin susceptibility,

$$\mathrm{Re}\ \chi(\vec{q},\omega=0)\equiv\int_0^{\beta}\langle m_z(\vec{q},\tau)m_z(-\vec{q},0)\rangle,$$

$$m_z(\vec{q},\tau)=e^{\tau H}m_z(\vec{q})e^{-\tau H},$$

and

$$m_z(\vec{q})=\frac{1}{\sqrt{N}}\sum_{\vec{r}} e^{i\vec{q}\vec{r}}(n_{\vec{r},\uparrow}-n_{\vec{r},\downarrow}). \tag{40}$$

Before considering the superconducting phase, we briefly summarize the temperature dependence of Re $\chi(\vec{q},\omega=0)$ at wave vectors $\vec{q}=0$ and $\vec{q}=\vec{Q}\equiv(\pi,\pi)$ for the Hubbard model at $U/t=4$. The results are plotted in Fig. 8. One expects the physics of the half-filled Hubbard model to be well described by a Heisenberg model in the renormalized classical regime.[34] Hence, an exponential divergence of Re $\chi(\vec{Q},\omega=0)$ as a function of temperature is expected. The data [see Fig. 8(b)] show a sharp increase at a temperature scale $T\sim 0.25t$. We use this criterion to define the magnetic energy scale $J\sim 0.25t$ at $W/t=0$. At temperatures $T>J$ the uniform static susceptibility Re $\chi(\vec{q}=0,\omega=0)$ increases monotonically with decreasing temperature. In this temperature regime, the overall scale of Re $\chi(\vec{q}=0,\omega=0)$, is greater than its free-electron value. This enhancement can be understood by the Stoner enhancement in the RPA approximation. In the low-temperature limit Re $\chi(\vec{q}=0,\omega=0)$ scales to a finite value due to the existence of gapless spin-wave excitations. One notices that Re $\chi(\vec{q}=0,\omega=0)$ shows a maximum at approximately $T\sim J$.

At $W/t=0.35$ Re $\chi(\vec{Q},\omega=0)$ diverges in the low temperature limit [see Fig. 9(b)]. This divergence is weaker than at $W/t=0$, and reflects the slow decay of the real-space spin-spin correlations. In the superconducting state the spin stiffness vanishes, and one expects a power-law divergence of Re $\chi(\vec{Q},\omega=0)$ as a function of temperature. From these data, we may identify a magnetic-energy scale $J\sim 0.5t$ at $W/t=0.35$. Being a local quantity, J is to first approximation insensitive to lattice size. That J is greater at $W/t=0.35$ than at $W/t=0$ may be seen by inspecting the nature of the added interaction H_W. In the Introduction, we have argued that at finite values of U/t, the relevant physics contained in the H_W term is given by $H_W^{(4)}$ in Eq. (6). As noted, $H_W^{(4)}$ contain terms of the form $-W\Delta^{\dagger}_{\vec{i},\delta}\Delta_{\vec{i},\delta}$, which may be written as $W(\vec{S}_{\vec{i}}\cdot\vec{S}_{\vec{i}+\vec{\delta}}-\frac{1}{4}n_{\vec{i}}n_{\vec{i}+\vec{\delta}})$. This term explicitly enhances the value of J. At $W/t=0.35$, and over the entire considered temperature region, Re $\chi(\vec{q}=0,\omega=0)$ is suppressed in comparison to its free-electron value [see Fig. 9(a)]. We interpret this overall suppression as a signature of pairing fluctuations. For our two largest lattice sizes, $L=6$ and $L=8$, Re $\chi(\vec{q}=0,\omega=0)$ shows a maximum at $T\sim 0.5t$, which coincides with our previously determined J scale. The fact that this maximum does not scale with system size (at least for our two largest lat-

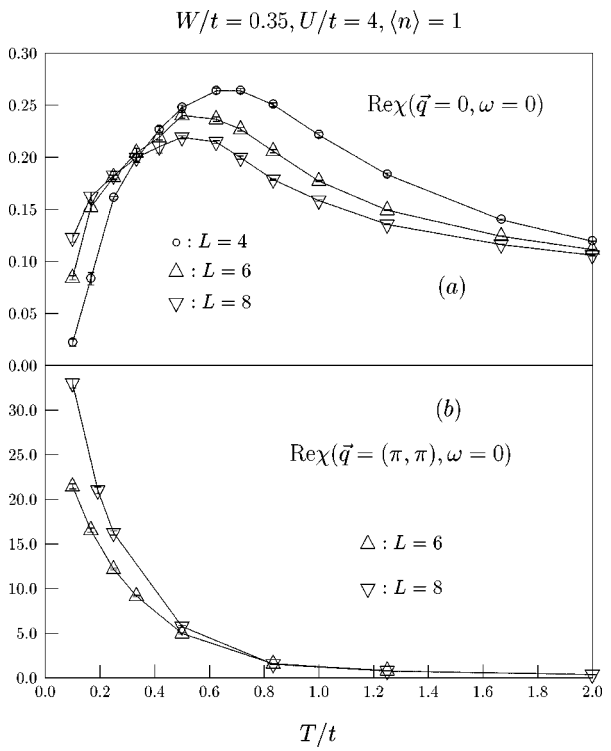

FIG. 9. (a) Uniform (b) staggered static spin susceptibility in the superconducting state at $W/t=0.35$ and $U/t=4$. The calculations were carried out at $\Phi=0$ [see Eq. (3)].

tices) makes us believe that it is related to the J scale and not to T_{KT}. In the low-temperature limit, and as expected for a superconducting state, the QMC data are consistent with the vanishing of Re $\chi(\vec{q}=0,\omega=0)$. We note that in BCS theory and for a $d_{x^2-y^2}$ order parameter, one obtains Re $\chi(\vec{q}=0,\omega=0)\sim T$ in the low-temperature limit.

T_{KT} is determined by using different boundary conditions [see Eq. (31)] than Re $\chi(\vec{q},\omega=0)$, which we calculate at $\Phi=0$ [see Eq. (3)]. Hence care has to be taken when comparing those two quantities. Strictly speaking, one should extrapolate the two data sets to the thermodynamic limit and only then compare. This is especially true in our case, since the size effects are strong in the determination of T_{KT} [see Eq. (35)]. We have seen that T_{KT} scales to $0.2t$ in the thermodynamic limit. At this temperature scale, no evident anomaly appears with growing lattice size in the QMC data in Fig. 9.

We now consider the dynamical structure factor:

$$S(\vec{q},\omega)=\frac{\mathrm{Im}\ \chi(\vec{q},\omega)}{1-e^{-\beta\omega}}, \tag{41}$$

where

$$\chi(\vec{q},\omega)=-i\int_0^\infty dt e^{i(\omega+i\delta)t}\langle[m_z(\vec{q},t),m_z(-\vec{q},0)]\rangle$$

and

$$m_z(\vec{q},t)=e^{itH}m_z(\vec{q})e^{-itH}. \tag{42}$$

In the above, we have set $\hbar=1$ and δ is a positive infinitesimal number. Im $\chi(\vec{q},\omega)$ is obtained by analytically continuing the imaginary time QMC data with the use of the classic maximum entropy method. We have used a flat default model for $S(\vec{q},\omega)$ and imposed the sum rules:

$$\int_{-\infty}^{\infty}d\omega\ \frac{\mathrm{Im}\ \chi(\vec{q},\omega)}{\omega}=\pi\ \mathrm{Re}\ \chi(\vec{q},\omega=0),$$

$$\int_{-\infty}^{\infty}d\omega\ \mathrm{Im}\ \chi(\vec{q},\omega)\coth(\beta\omega/2)=2\pi\langle m_z(\vec{q})m_z(-\vec{q})\rangle,$$

and

$$\int_{-\infty}^{\infty}d\omega\ \mathrm{Im}\ \chi(\vec{q},\omega)\omega=\pi\langle[m_z(-\vec{q}),[H,m_z(\vec{q})]]\rangle. \tag{43}$$

Figure 10 plots $S(\vec{Q},\omega)$ as a function of temperature at $W/t=0.35$ on 6×6 and 8×8 lattices. For comparison, we have plotted at the lowest considered temperature, $\beta=0.1t$, $S(\vec{Q},\omega)$ for the Hubbard model (i.e., $W/t=0$). $S(\vec{q},\omega)$ satisfies the sum rule:

$$\int_{-\infty}^{\infty}d\omega S(\vec{q},\omega)=\pi\langle m_z(\vec{q})m_z(-\vec{q})\rangle\equiv\pi S(\vec{q}). \tag{44}$$

At $W/t=0$, $S(\vec{Q})$ diverges as L^2 in the zero temperature limit. This weight is centered at $\omega=0$. At $W/t=0.35$, and at a scale set by $J\sim0.5t$, we observe a buildup of spectral weight centered around $\omega=0$. At a lower-temperature scale, which we will identify below, spectral weight is shifted from lower frequencies to form a peak at finite frequency. Defining ω_0 by the peak value of $S(\vec{Q},\omega)$ at the lowest considered temperature, we see that $\omega_0/T_{\mathrm{KT}}\sim0.4$. This relation is valid for both considered lattice sizes. Since the equal time spin-spin correlations in the superconducting state decay slower than $\cos(\vec{Q}\vec{r})/|\vec{r}|^2$ at zero temperature, the spectral weight under the peak at ω_0 diverges in the thermodynamic and low-temperature limits.

The relaxation rate we consider is defined by

$$\frac{1}{T_1T}=\lim_{\omega\to0}\frac{1}{N}\sum_{\vec{q}}\ \frac{\mathrm{Im}\ \chi(\vec{q},\omega)}{\omega}, \tag{45}$$

where a $\vec{q}$-independent nuclear form factor is assumed. Figure 11 plots $1/T_1$ both in the superconducting and antiferromagnetic insulating state. The *error bars* are obtained in the following way. Let v_τ be a set of imaginary time data, and $C_v(\tau,\tau_1)$ the accompanying covariance matrix. Here $\tau,\tau_1:1,\ldots,m$. In the basis where the covariance matrix is diagonal, $U^\dagger C_v U=\mathrm{diag}(d_1,\ldots,d_m)$, we can add independent noise to the data in the following way: $\vec{v}_{\vec{\eta}}=U(U^\dagger\vec{v}+\vec{\eta})$ where η_τ are Gaussian distributed random variables satisfying $\langle\eta_\tau\rangle=0$ and $\langle\eta_\tau\eta_{\tau'}\rangle=\delta_{\tau,\tau'}d_\tau$. We carry out the analytical continuation with the data set $\vec{v}_{\vec{\eta}}$ and repeat the procedure for several realizations of $\vec{\eta}$. The *error bars* in Fig. 11 correspond to the variance of the so-obtained values of $1/T_1$. $1/T_1$ is a delicate quantity to compute with QMC methods. To check the reliability of our calculations we first consider the $W/t=0$ case. At temperatures $T<J$ as determined from Re $\chi(\vec{Q},\omega=0)$, an increase in $1/T_1$ is observed.

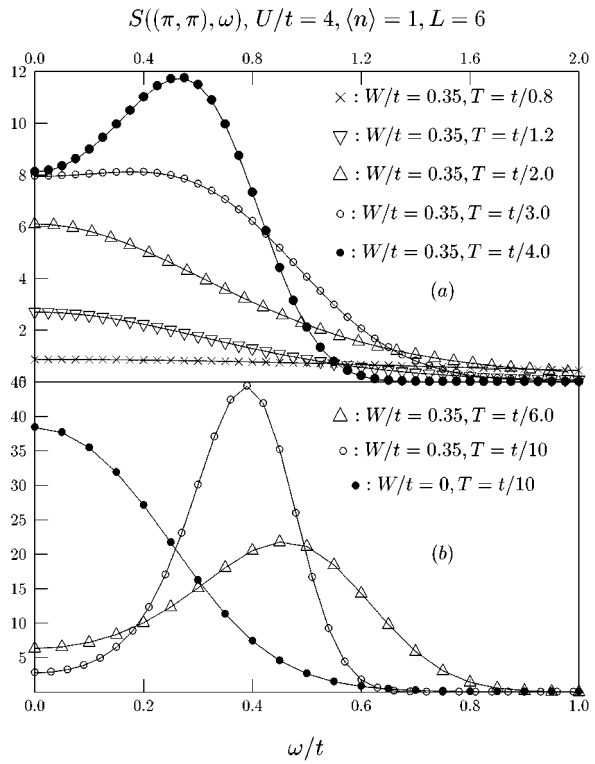

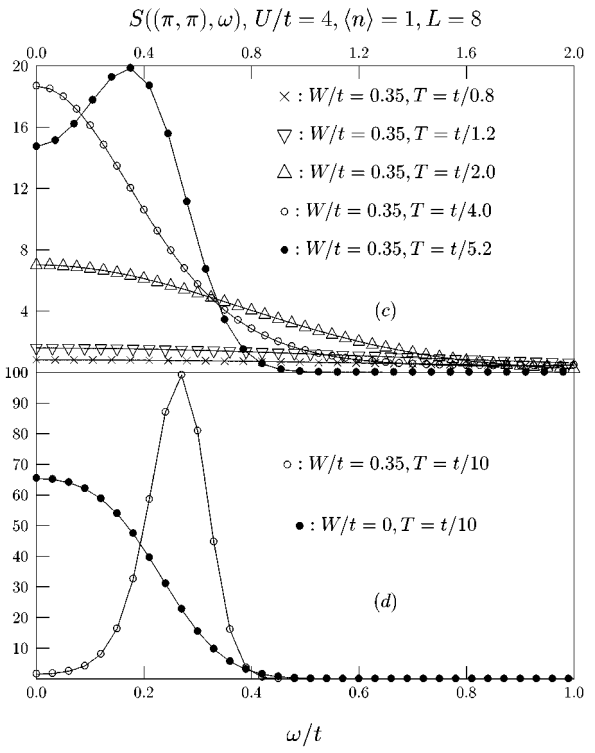

FIG. 10. $S(\vec{Q},\omega)$ in the superconducting state at $W/t=0.35$, $U/t=4$ as a function of system size and temperature. For comparison, at the lowest considered temperature, $T=0.1t$, we have included the result for the Hubbard model (i.e., $W/t=0$) at $U/t=4$. Here, $\Phi=0$ [see Eq. (3)].

This is an expected feature since in the renormalized classical regime of quantum antiferromagnets, $1/T_1$ diverges exponentially with decreasing temperature.[34] In the superconducting state at $W/t=0.35$, we plot $1/T_1$ as a function of

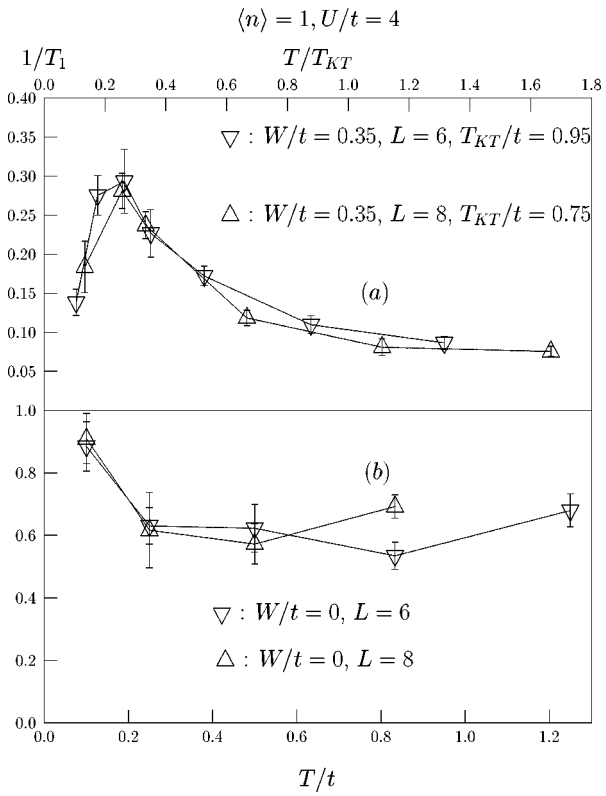

FIG. 11. (a) $1/T_1$ vs T/T_{KT} in the superconducting state at $W/t=0.35$. The magnetic scale is given by $J\sim 0.5t$. In the thermodynamic limit, $T_{\mathrm{KT}}\sim 0.2t$ and J is to first approximation size independent. Thus $J/T_{\mathrm{KT}}\sim 2.5$ at $L\rightarrow\infty$. (b) $1/T_1$ vs T for the antiferromagnetic Mott insulating state. Here, $J\sim 0.25t$. The calculations were carried out at $\Phi=0$ [see Eq. (3)].

T/T_{KT} [see Fig. 11(a)]. The overall scale of $1/T_1$ is reduced in the superconducting state as compared to the antiferromagnetic Mott insulating state. For both considered lattice sizes, $1/T_1$ shows a maximum at $T\sim 0.25T_{\mathrm{KT}}$ which allows us to define a crossover temperature scale: $T_1^{\mathrm{cr}}/T_{\mathrm{KT}}\sim 0.25$. At temperatures lower than T_1^{cr}, the QMC data are consistent with the vanishing of the relaxation rate $1/T_1$. In BCS theory with a $d_{x^2-y^2}$ order parameter, $1/T_1\sim T^3$ in the low-temperature limit. At temperatures above T_1^{cr}, $1/T_1$ grows with decreasing temperature. One expects $1/T_1$ to start increasing at the magnetic scale J as determined from Re $\chi(\vec{Q},\omega=0)$. Since in Fig. 11(a) we set the temperature scale by T_{KT} large size effects are now present in J/T_{KT}, which takes the values 0.5 (0.65) for the $L=6$ ($L=8$) lattice and scales to $J/T_{\mathrm{KT}}\sim 2.5$ in the thermodynamic limit. The so-determined crossover temperature coincides well with the temperature scale at which spectral weight in $S(\vec{Q},\omega)$ is shifted from low frequencies to form the peak centered at ω_0 (see Fig. 10).

V. SUMMARY AND CONCLUSIONS

As schematically illustrated in Fig. 12(a) our zero temperature results at $U/t=4$ are best summarized in the $W-\mu$ plane where μ denotes the chemical potential. We have carried out our simulations at half-filling, $\mu=0$, and shown the occurrence of a quantum transition between an antiferro-

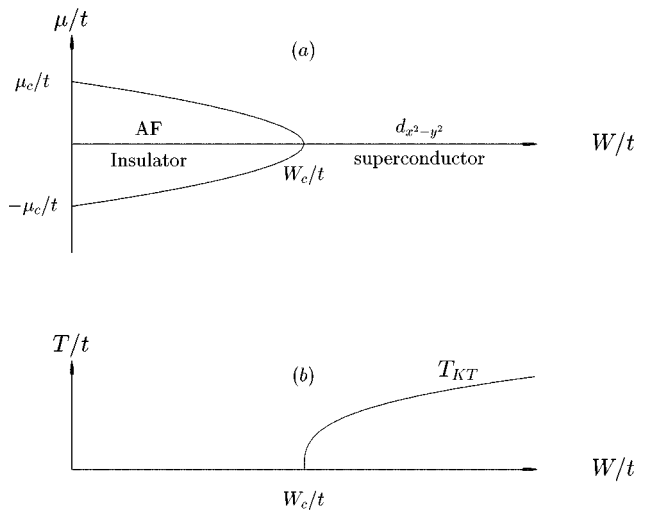

FIG. 12. (a) Schematic phase diagram of the model $H=H_U+H_W-\mu\hat{N}$ at zero temperature and in the $W-\mu$ [see Eq. (5)]. Here, μ corresponds to the chemical potential and $\hat{N}$ is the particle number operator. Half-filling corresponds to $\mu=0$. At $U/t=4$, $\mu=0$, we estimate $W_c/t\sim 0.3$ and $\mu_c/t=0.67\pm 0.015$ (Ref. 8). (b) Schematic phase diagram of $H=H_U+H_W$ in the T-W plane where T denotes the temperature. At $U/t=4$ and $W/t=0.35$ we estimate $T_{\mathrm{KT}}\sim 0.2t$.

magnetic Mott insulator and $d_{x^2-y^2}$ superconductor as a function of W/t. Within our numerical accuracy, the quantum transition occurs simultaneously in both the charge and spin degrees of freedom at $W_c/t\sim 0.3$. Although the spin stiffness vanishes in the superconducting state, the antiferromagnetic spin correlations decay slower than $1/|\vec{r}|^2$ where $|\vec{r}|$ denotes the distance. In two dimensions, this slow decay leads to a divergence of the equal-time spin structure factor at wave vector $\vec{Q}=(\pi,\pi)$. This feature shows the extreme compatibility of antiferromagnetic fluctuations and $d_{x^2-y^2}$ superconductivity. To a first approximation, the exponent of the power-law decay of the spin-spin correlations varies with the coupling strength W/t. At $W/t=0.6$ the QMC data for lattice sizes ranging from $L=4$ to $L=16$ are consistent with real-space spin-spin correlations of the form $\cos(\vec{Q}\vec{r})/|\vec{r}|^{-\alpha}$ with $\alpha\sim 1.16$. The QMC data suggest that α decreases continuously to $\alpha=1$ as the coupling W/t approaches W_c/t. Hence, $W_c/t\sim 0.3$ terminates a critical line in the schematic phase diagram drawn in Fig. 12(a).

As a natural consequence of Fig. 12(a) we expect at $W<W_c$ a doping induced quantum transition between an antiferromagnetic Mott insulator and $d_{x^2-y^2}$ superconductor. As mentioned in the Introduction, the anomalous compressibility and unusually large dynamical exponent observed numerically at the filling controlled metal-insulator transition.[6–8] enhances the sensitivity of the system to two-particle processes as generically contained in the form H_W. Work along those lines, for the filling controlled transition, is in progress.

To determine the order of the phase transition at W_c/t is presently beyond the reach of our numerical calculations. At the mean field level, the transition is expected to be of first order since the phases have different broken symmetries. In this scenario, the staggered moment would be expected to show a jump at the critical coupling constant. Within our numerical accuracy, we do not observe such a feature, and the possibility of a continuous phase transition remains open. An example of a continuous phase transition between two broken symmetry states on a square lattice is found in the case of quantum antiferromagnets where the Berry phase is a dangerously irrelevant operator that leads to spin-Peierls ordering (i.e., broken lattice symmetry) in the disordered state for half-integer spin.[35–37]

In the κ-type BEDT-TTF compounds, the antiferromagnetic and superconducting phases are adjacent to each other in the plane of temperature and either pressure, anion substitution, or deuteration of hydrogen atoms.[38–40] Thus both changes in the bandwidth and in the interaction strength have been studied. The insulating phase of the κ-type BEDT-TTF compounds is a correlated insulator in the sense that band-structure calculations predict a metal.[41] A dimer model has been proposed to account for the magnetic insulating phase.[38] Here, a pair of BEDT-TTF molecules carries a charge of unity, and constitute a single site in terms of a Hubbard model. The *on-site* Hubbard interaction U_{dimer} depends upon the intradimer hopping, t_{dimer}. In the limit of large Coulomb repulsion per BEDT-TTF molecule, $U_{\mathrm{dimer}}\sim t_{\mathrm{dimer}}$. Because of the layered structure of this compound, our two-dimensional model may offer a simplified description of the system. In those compounds, the direct transition line between the antiferromagnetic and superconducting phases appears to extend to finite temperatures, thus implying a first-order phase transition. A detailed comparison between theory and experiment is beyond the scope of this work. However, an interesting point is that in the superconducting phase both our results and experimental results show a common feature: the peak temperature in Re $\chi(\vec{q}=0,\omega=0)$ is higher than the crossover temperature in $1/T_1$ (i.e., T_1^{cr} in our notation). It would be interesting to see whether the antiferromagnetic fluctuations are robust [i.e., divergence of Re $\chi(\vec{Q},\omega=0)$] in the superconducting phase. We also note that the ^{13}C nuclear spin relaxation rate in the superconducting phase of the κ-type BEDT-TTF compounds has been reported to follow a T^3 law,[42] which would be consistent with a $d_{x^2-y^2}$ order parameter.

We have studied spin and charge degrees of freedom at finite temperatures in the superconducting phase, at coupling strength $W/t=0.35$. As schematically drawn in Fig. 12(b) we expect the occurrence of a finite-temperature Kosterlitz-Thouless transition. We give numerical evidence that such a transition indeed occurs. After extrapolation to the thermodynamic limit we estimate $T_{\mathrm{KT}}\sim 0.2t$ at $W/t=0.35$. In the vicinity of the Kosterlitz-Thouless transition temperature a pseudogap in the one-electron density of states, $N(\omega)$, appears. On our finite-sized lattices, the pseudogap feature appears above T_{KT}. For the three considered lattice, $L=6$, $L=8$, and $L=10$, the estimated superconducting gap scales as T_{KT} and satisfies $\Delta_{\mathrm{sc}}/T_{\mathrm{KT}}\sim 2.5$.

In the superconducting phase, at $W/t=0.35$, Re $\chi(\vec{Q},\omega=0)$ diverges in the low-temperature and thermodynamic limits. This divergence as a function of temperature is slower than in the antiferromagnetic Mott insulating state at $W/t=0$, and is expected to follow a power law. We may estimate a magnetic scale by the temperature at which Re $\chi(\vec{Q},\omega=0)$

starts to increase. At $W/t=0.35$, we obtain $J\sim 0.5t$. The QMC data are consistent with the vanishing of Re $\chi(\vec{q}=0,\omega=0)$ in the zero-temperature and thermodynamic limits. Re $\chi(\vec{q}=0,\omega=0)$ shows a maximum at $T\sim J$. A similar although stronger feature is seen in the Hubbard model (i.e., $W/t=0$). From the relaxation rate $1/T_1$, we estimate a crossover temperature, $T_1^{\rm cr}$ below which $1/T_1$ decreases. This temperature scale satisfies $T_1^{\rm cr}/T_{\rm KT}\sim 0.25$. In the temperature range $T_1^{\rm cr}<T<J$, $1/T_1$ grows with decreasing temperature. At the temperature scale set by $T_1^{\rm cr}$ spectral weight in $S(\vec{Q},\omega)$ is shifted from low frequencies to form a peak at ω_0. The location of the peak ω_0 scales with $T_{\rm KT}$ as a function of system size and satisfies $\omega_0/T_{\rm KT}\sim 0.4$. The spectral weight under this peak diverges in the zero-temperature and thermodynamic limits.

The superconducting state at $W/t=0.35$ is thus best characterized by (i) the divergence of Re $\chi(\vec{Q},\omega=0)$, but the vanishing of $1/T_1$ in the low-temperature and thermodynamic limits and (ii) $\omega_0/\Delta_{\rm sc}\sim 0.15\ll 1$. This behavior is nontrivial and points to the extreme compatibility of $d_{x^2-y^2}$ superconductivity and antiferromagnetic spin fluctuations.

To conclude, the here-presented model shows a rich phase diagram. The doping of the model offers the possibility of reproducing some of the features of the cuprates at an energy scale accessible to numerical simulations.

ACKNOWLEDGMENTS

We thank N. Bulut, T. Dahm, W. Hanke, T. Mueller, M. Randeria, S. Sachdev, A. Sandvik, and S. C. Zhang for instructive conversations. The numerical simulations were carried out on the FACOM VPP500 at the Supercomputer Center of the Institute for Solid State Physics, University of Tokyo. F.F.A thanks the Swiss National Science Foundation for financial support under Grant No. 8220-042824. D.J.S. and F.F.A. acknowledge partial support from the National Science Foundation under Grant No. DMR95-27304. M.I. thanks the Institute of Theoretical Physics at the University of California, Santa Barbara for hospitality. M.I. acknowledges financial support from the National Science Foundation under the Grant No. PHY94-07194 as well as from a Grant-in-Aid for Scientific Research on the Priority Area ''Anomalous Metallic States near the Mott Transition'' and ''Novel Electronic States in Molecular Conductors'' from the Ministry of Education, Science and Culture, Japan.

APPENDIX A: TRIAL WAVE FUNCTIONS FOR THE PQMC

In this appendix we show how to construct trial wave functions that generate no sign problem if $N^{\uparrow}+N^{\downarrow}=N$, and in the special case, $N^{\uparrow}=N^{\downarrow}=N/2$ are spin singlets. We provide explicit forms of the trial wave functions used in this work. Our starting point is the noninteracting Hamiltonian:

$$H_0=\sum_{\vec{i},\vec{j}} c_{\vec{i}}^{\dagger}T_{\vec{i},\vec{j}}c_{\vec{j}}. \tag{A1}$$

H_0 corresponds to the Hamiltonian (5) in the limit $U=W=0$. We have omitted the spin index, and consider the boundary condition given by Eq. (3). Let U be the unitary transformation that diagonalizes T: $U^{\dagger}TU=\mathrm{diag}(\lambda_1,\ldots,\lambda_N)$. We define the hole operators by $h_{\vec{i}}=(-1)^{\vec{i}}c_{\vec{i}}^{\dagger}$ as well as

$$\gamma_{\vec{k}}=\sum_{\vec{i}} U_{\vec{k},\vec{i}}^{\dagger}c_{\vec{i}} \quad\text{and}\quad \eta_{\vec{k}}=\sum_{\vec{i}} h_{\vec{i}}(-1)^{\vec{i}}U_{\vec{i},\vec{k}}. \tag{A2}$$

We have used the notation $(-1)^{\vec{i}}=(-1)^{i_x+i_y}$. The above operators satisfy

$$[H_0,\gamma_{\vec{k}}^{\dagger}]=\lambda_{\vec{k}}\gamma_{\vec{k}}^{\dagger} \quad\text{and}\quad [H_0,\eta_{\vec{k}}^{\dagger}]=-\lambda_{\vec{k}}\eta_{\vec{k}}^{\dagger}. \tag{A3}$$

We set the trial wave function in the up-spin sector to be the ground state of H_0: $|\Psi_T^{\uparrow}\rangle=\Pi_{\vec{k}\epsilon A}\gamma_{\vec{k}}^{\dagger}|0\rangle$, where $|0\rangle$ is the electron vacuum and A is set of $\vec{k}$ points defined by the requirement that $|\Psi_T\rangle$ is the ground state of H_0. By construction $|\Psi_T^{\uparrow}\rangle=\Pi_{\vec{k}\epsilon\bar{A}}\eta_{\vec{k}}^{\dagger}|0^h\rangle$, where $|0^h\rangle$ is the hole vacuum and $\bar{A}$ is the complement of A. We may hence define

$$P_{\vec{i},\vec{k}}^{\uparrow}=U_{\vec{i},\vec{k}}, \quad \vec{i}:1,\ldots,N, \quad \vec{k}\epsilon A,$$

$$P_{\vec{i},\vec{k}}^{\downarrow}=(-1)^{\vec{i}}\bar{U}_{\vec{i},\vec{k}}, \quad \vec{i}:1,\ldots,N, \quad \vec{k}\epsilon\bar{A}. \tag{A4}$$

With this choice of P^{σ} no sign problem occurs [see Eqs. (18), (23), (24), and (25)]. We note that the only restriction on the particle number is $N^{\uparrow}+N^{\downarrow}=N$.

In the special case $N^{\uparrow}=N^{\downarrow}=N/2$ the trial wave function $|\Psi_T\rangle=|\Psi_T^{\uparrow}\rangle\otimes|\Psi_T^{\downarrow}\rangle$ satisfies

$$\sum_{i,j}\langle\Psi_T|\vec{S}_{\vec{i}}\cdot\vec{S}_{\vec{j}}|\Psi_T\rangle=\frac{1}{2}\sum_{\vec{k}} f^{\gamma}(\vec{k})f^{\eta}(\vec{k}) + [f^{\gamma}(\vec{k})-1][f^{\eta}(\vec{k})-1],$$

where

$$f^{\eta}(\vec{k})=\langle\Psi_T^{\downarrow}|\eta_{\vec{k}}^{\dagger}\eta_{\vec{k}}|\Psi_T^{\downarrow}\rangle \quad\text{and}\quad f^{\gamma}(\vec{k})=\langle\Psi_T^{\uparrow}|\gamma_{\vec{k}}^{\dagger}\gamma_{\vec{k}}|\Psi_T^{\uparrow}\rangle. \tag{A5}$$

If the ground state of H_0 with $N/2$ particles per spin sector is nondegenerate, then $\Sigma_{\vec{i},\vec{j}}\langle\Psi_T|\vec{S}_{\vec{i}}\cdot\vec{S}_{\vec{j}}|\Psi_T\rangle$ vanishes, independently of the choice of the unitary transformation U. For nonzero values of the flux Φ (i.e., $\Phi\neq 2\pi n\Phi_0$, n being an integer), this condition is satisfied, and hence a trial wave function showing no sign problem and satisfying Eq. (26), may easily be constructed numerically.

At $\Phi=0$, the ground state of H_0 with $N/2$ particles per spin sector is degenerate, and the total spin of the trial wave function will depend on the choice of the unitary transformation U. In principle, one can use the trial wave function obtained at an *infinitesimal* value of Φ to lift the degeneracy. This procedure would force us to work with complex num-

bers that enhances the CPU time by a factor of 3–4. To easily circumvent those problems we define a new Hamiltonian,

$$\begin{aligned}\tilde{H}_0 = &-t(1-\delta)\sum_{\vec{i}} (c^{\dagger}_{\vec{i}} c_{\vec{i}+\vec{a}_y} + \text{H.c.}) \\ &-t(1-\delta)\sum_{\vec{i}=(2i_x+1,i_y)} (c^{\dagger}_{\vec{i}} c_{\vec{i}+\vec{a}_x} + \text{H.c.}) \\ &-t(1+\delta)\sum_{\vec{i}=(2i_x,i_y)} (c^{\dagger}_{\vec{i}} c_{\vec{i}+\vec{a}_x} + \text{H.c.}) \qquad \text{(A6)}\end{aligned}$$

with periodic boundary conditions in both lattice directions. For *infinitesimal* values of δ, the ground state of $\tilde{H}_0$ with $N/2$ particles is nondegenerate. Diagonalizing $\tilde{H}_0$ generates an orthogonal matrix U from which one may construct the trial wave function. Both for the here-presented model (see Fig. 2) and for the half-filled Hubbard model,[17] the above trial wave functions provide quick convergence to the ground state. The reason lies in the fact that they are spin singlets and hence orthogonal to spin-wave excitations, which constitute the low-energy part of the spectrum at least in the case of the half-filled Hubbard model.

*Present address: Institut für Theoretische Physik III, Universität Stuttgart, Pfaffenwaldring 57, D-70550 Stuttgart, Germany.

[1] For a review, see D. J. Scalapino, in *Does the Hubbard model have the right stuff?,* Proceedings of the International School of Physics, Enrico Fermi, Course CXXI, edited by R. A. Broglia and J. R. Schrieffer (North-Holland, Amsterdam, 1994), and references therein.
[2] F. F. Assaad, M. Imada, and D. J. Scalapino, Phys. Rev. Lett. **77**, 4592 (1996).
[3] W. P. Su, J. R. Schrieffer, and A. J. Heeger, Phys. Rev. B **22**, 2099 (1980).
[4] J. E. Hirsch, Phys. Rev. B **35**, 8726 (1987).
[5] M. Imada, Prog. Theor. Phys. Suppl. **113**, 203 (1993).
[6] M. Imada, J. Phys. Soc. Jpn. **64**, 2954 (1995).
[7] N. Furukawa and M. Imada, J. Phys. Soc. Jpn. **62**, 2557 (1993); N. Furukawa, F. F. Assaad, and M. Imada, *ibid.* **65**, 2339 (1996).
[8] F. F. Assaad and M. Imada, Phys. Rev. Lett. **76**, 3176 (1996).
[9] N. Bulut, D. J. Scalapino, and S. R. White, Phys. Rev. B **47**, 6157 (1993); **47**, 14 599 (1993).
[10] R. Blankenbecler and R. L. Sugar, Phys. Rev. D **27**, 1304 (1983).
[11] G. Sugiyama and S. E. Koonin, Ann. Phys. (N.Y.) **168**, 1 (1986).
[12] S. Sorella, S. Baroni, R. Car, and M. Parrinello, Europhys. Lett. **8**, 663 (1989); S. Sorella, E. Tosatti, S. Baroni, R. Car, and M. Parinello, Int. J. Mod. Phys. B **1**, 993 (1989).
[13] M. Imada and Y. Hatsugai, J. Phys. Soc. Jpn. **58**, 3752 (1989).
[14] J. E. Hirsch, Phys. Rev. B **31**, 4403 (1985).
[15] S. R. White *et al.*, Phys. Rev. B **40**, 506 (1989).
[16] F. F. Assaad, W. Hanke, and D. J. Scalapino, Phys. Rev. B **50**, 12 835 (1994).
[17] F. F. Assaad and M. Imada, J. Phys. Soc. Jpn. **65**, 189 (1996).
[18] R. M. Fye, Phys. Rev. B **33**, 6271 (1986).
[19] J. E. Hirsch, Phys. Rev. B **28**, 4059 (1983).
[20] E. Loh and J. Gubernatis, in *Modern Problems of Condensed Matter Physics*, edited by W. Hanke and Y. V. Kopaev (North Holland, Amsterdam, 1992), Vol. 32, p. 177.
[21] M. Jarrel and J. E. Gubernatis, Phys. Rep. **269**, 133 (1996).
[22] W. von der Linden, Appl. Phys. A: Mater. Sci. Proc. **60**, 155 (1995).
[23] W. Kohn, Phys. Rev. **133**, A171 (1964).
[24] N. Byers and C. N. Yang, Phys. Rev. Lett. **7**, 46 (1961).
[25] C. N. Yang, Rev. Mod. Phys. **34**, 694 (1962).
[26] F. F. Assaad, W. Hanke, and D. J. Scalapino, Phys. Rev. Lett. **71**, 1915 (1993).
[27] J. M. Kosterlitz and D. J. Thouless, J. Phys. C **6**, 1181 (1973).
[28] D. R. Nelson and J. M. Kosterlitz, Phys. Rev. Lett. **39**, 1201 (1977).
[29] J. E. Van Himbergen and S. Chakravarty, Phys. Rev. B **23**, 359 (1981).
[30] E. Loh, Jr., D. J. Scalapino, and P. M. Grant, Phys. Rev. B **31**, 4712 (1985).
[31] F. F. Assaad, W. Hanke, and D. J. Scalapino, Phys. Rev. B **49**, 4327 (1994).
[32] S. R. White, D. J. Scalapino, R. L. Sugar, N. E. Bickers, and R. T. Scalettar, Phys. Rev. B **39**, 839 (1989).
[33] N. Bulut and D. J. Scalapino, Phys. Rev. B **45**, 2371 (1992).
[34] S. Chakravarty, B. I. Halperin, and D. R. Nelson, Phys. Rev. Lett. **60**, 1057 (1988); Phys. Rev. B **39**, 2344 (1989).
[35] A. Chubukov, S. Sachdev, and J. Ye, Phys. Rev. B **49**, 11 919 (1994).
[36] N. Read and S. Sachdev, Phys. Rev. B **42**, 4568 (1990).
[37] Although we have used the SU(2) language, this result is derived in the large N limit of SU(N) quantum antiferromagnets.
[38] K. Miyagawa, A. Kawamoto, Y. Nakazawa, and K. Kanoda, Phys. Rev. Lett. **75**, 1174 (1995).
[39] A. Kawamoto, K. Miyagawa, Y. Nakazawa, and K. Kanoda, Phys. Rev. B **52**, 15 522 (1995).
[40] H. Ito, T. Ishiguro, M. Kubota, and G. Saito, J. Phys. Soc. Jpn. **65**, 1987 (1996).
[41] J. M. Williams *et al.*, Science **252**, 1501 (1991), and references therein.
[42] K. Kanoda, K. Miyagawa, A. Kawamoto, and Y. Nakazawa, Phys. Rev. B **54**, 76 (1996).